

Buckled honeycomb group-V - S_6 symmetric $(d - 2)$ higher order topological insulators

Santosh Kumar Radha* and Walter R. L. Lambrecht†
*Department of Physics, Case Western Reserve University,
 10900 Euclid Avenue, Cleveland, OH-44106-7079*

Higher Order Topological Insulators (HOTI) are d -spatial dimensional systems featuring topologically protected gap-less states at their $(d - n)$ -dimensional boundaries. With the help of *ab-initio* calculations and tight binding models along with symmetry considerations we show that monolayer buckled honeycomb structures of group-V elements (Sb,As), which have already been synthesized, belong in this category and have a charge fractionalization of $\frac{e}{2}$ at the corner states as well as weak topological edge states, all protected by their properties under the inversion operation which classify this system as a quadrupole topological insulator.

Since the discovery of topological insulators (TIs), various exotic topological phases of matter have been discovered. A new class of such systems are higher-order topological insulators (HOTIs). Unlike regular TIs, n^{th} order HOTIs have protected edge states in their corresponding $(d - n)$ dimension, where $d > n > 1$. [1–5] Various 3D materials [5–9] and artificial systems [10–14] have recently been proposed to be HOTIs. It was recently also proposed that gap-less HOTI boundary states in proximity to a superconductor could host Majorana states without the need for special pairing mechanisms or magnetic fields. [15]

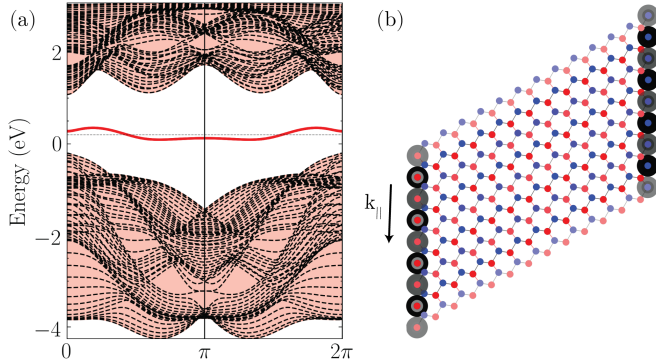


FIG. 1: (a) Density functional theory band structure of nanoribbon of buckled monolayer Sb in local density approximation along the zigzag edge \mathbf{k}_{\parallel} , showing edge states (red); (b) structure and edge state wave function modulo squared.

In this letter, we show that an already existing 2D material system - monolayer buckled honeycomb β -Sb [16] is a $n = 2$ HOTI that is protected by S_6 symmetry. Our symmetry analysis closely follows and slightly generalizes the model introduced by Ref [17] for C_n -symmetric systems. We will furthermore show that it is closely related to, but not identical to, the Kekulé lattice, *i.e.* a honeycomb lattice with bond alternation. In this system both weak edge states occur in 1D nanoribbons and corner states in 0D fragments of the lattice and are related

to the quadrupole character of the system as defined in Refs. 1 and 4.

Background on monolayer Sb - In a recent paper [18], we studied the topological behavior of honeycomb monolayer Sb from the completely flat to the free-standing equilibrium buckled structure. In that paper we showed that unlike in graphene, the s -states of Sb form essentially decoupled separate bands from the p -orbitals because of their energy separation in the atom. While in the (nearly) flat honeycomb structure, p_z orbitals are also (nearly) decoupled from the p_x, p_y orbitals by the horizontal mirror plane, the set of three p -orbitals in the equilibrium buckled structure can fully interact and form bonding and antibonding sets of bands separated by a gap and thus this system was until now considered a trivial semiconductor. However, we found that relatively flat edge states occur in the middle of the gap of nanoribbons of the buckled form and point to another type of topological effect being responsible for these surface states. The density functional theory (DFT) band structure results for a nanoribbon are shown in Figure 1 as obtained from a tight-binding model parametrized with maximally localized Wannier function extracted hopping integrals from a projector augmented wave (PAW) [19] calculation of the 2D periodic system using the Quantum Espresso [20] and Wannier90 codes [21]. Computational details are given in Supplemental Material (SM). [22]

Qualitative discussion of origin of edge states - In a broad sense the origin of these edge states is related to the “obstructed atomic limit” (OAL), a concept introduced by Bradlyn *et al.* [23, 24]. Accordingly, a set of bands is in the OAL when they possess symmetric, localized Wannier functions that reside on Wyckoff positions distinct from the atomic positions which cannot be smoothly deformed to the latter. This corresponds to a weak topological phase.

In the present case, the bands of interest result from the Sb- $\{p_x, p_y, p_z\}$ orbitals which form three sets of bonding (occupied, valence) and three sets of antibonding (empty, conduction) bands. These bands are shown in Figure 2 along with the relevant symmetry labeling and indicating the atomic orbital character of each band.

This band structure is actually obtained at the quasiparticle self-consistent (QS)GW level[25] which guarantees accurate band gaps but for the remainder of this paper, this is not important and a DFT or even simpler tight-binding (TB) models have the same set of irreducible representations present in the valence (VB) and conduction (CB) band manifolds as shown in SM.[22].

Significant hybridization between all three p -orbitals is apparent. To better understand the origin of the gap and hybridization, we plot in Figure 2(b) the $\sum_{n\mathbf{k}} |\psi_{n\mathbf{k}}|^2$ separately for $n \in \text{VB}$ and CB manifolds. These show clearly that the Wannier function corresponding to the VB are localized at the bond centers, while the ones of the CB are centered at the “antibond centers”, obtained from the bond center by inversion about the atomic sites. This in itself is already a clear indicator of the non-trivial nature of the band structure. Intuitively, if one cuts the system along these bonds, dangling bond like edge states are expected.

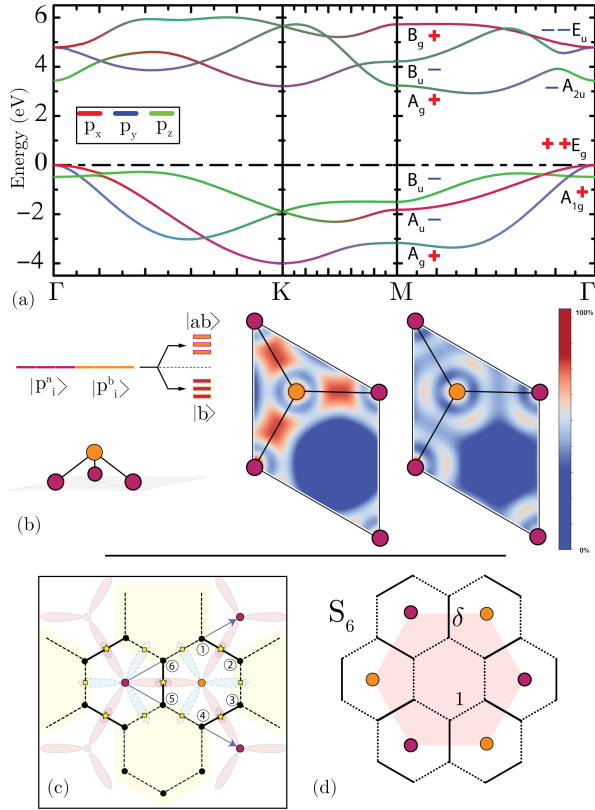


FIG. 2: (a) QSGW band structure of honeycomb-buckled Sb; (b) schematic of p -levels from atomic limit to buckled Sb and contour plot of total electron density from the 3 p -derived valence ($|b\rangle$) and conduction ($|ab\rangle$) bands; (c) relation of bond centers to Kekulé model: see text; (d) Kekulé model.

Relation to Kagome and Kekulé lattice - Remarkably the bond centers and antibond centers from respec-

tively a Kagome and *anti-Kagome* lattice as illustrated in SM.[22] More interestingly, a further transformation relates this band structure to the Kekulé lattice. As shown in Figure 2(c) the bond centers (yellow stars) of the (pink) bonding orbitals of Sb atoms (orange and red circles) and the corresponding antibond (blue) centers (yellow squares) can alternatively be viewed as the bond centers of yet another honeycomb lattice (black circles) with alternating bond strength. We may recognize this as the bond modulated honeycomb lattice, known as the Kekulé lattice. We can see in Figure 2(d) that this lattice consists of hexagon shaped molecules connected by (intracell) bonds of strength 1 within the Wigner-Seitz unit cell and connected by intercell bonds of strength δ . It is useful to note that the bond centers of the original buckled Sb lattice, which coincide with the bond centers of the final Kekulé lattice all lie in the same horizontal plane. The Kekulé lattice is thus strictly 2D and the inversion operator in 2D is identical with a two-fold rotation C_2 about the z -axis. Thus the point group of the Kekulé lattice is C_6 while that of the Sb lattice is S_6 but the two are simply related by replacing the C_2 operation by the inversion operation, which we will denote \mathcal{I} .

The topological properties of the Kekulé lattice have been discussed in a number of recent papers.[13, 26–29] These papers have not only shown the presence of topological edge states but also topological corner states in the Kekulé lattice in the nontrivial condition $\delta > 1$. Not surprisingly, one can think of Kekulé as a hexagonal 2D generalization of the Su-Schrieffer-Heeger (SSH) model[30] or a set of SSH models arranged next to each other.

Corner states - We now turn our attention to the higher order topologically required corner states in a 0D system that preserves the rotational symmetries of the periodic lattice, in other words, a finite hexagonal portion cut out from the buckled honeycomb lattice. First, let us mention that such hexagonal nanoflakes have already been fabricated[31]. Benalcazar *et al.* [17] have described topological invariants and the related occurrence of corner-states and their charge fractionalization for C_n groups. The conditions under which corner-states occur depend on the symmetries of the states at high-symmetry \mathbf{k} -points. While the system under study here has S_6 instead of C_6 symmetry, we can easily generalize their procedure. According to Benalcazar *et al.* [17] for the C_6 group, the topological invariant is $\chi^{(6)} = ([M_1^{(2)}], [K_1^{(3)}])$, which, for example at M indicates the difference in number of eigenstates in the occupied bands manifold of the C_2 operation indicated by the superscript corresponding to a given eigenvalues (1, the subscript) at M and Γ . A 6-fold rotation can be viewed as the product of a 3-fold and 2-fold rotation. Similarly, a 3-fold rotation-inversion is the product of a 3-fold rotation and an inversion. Thus we merely have to replace the two fold rotation by inversion for our case. Thus the im-

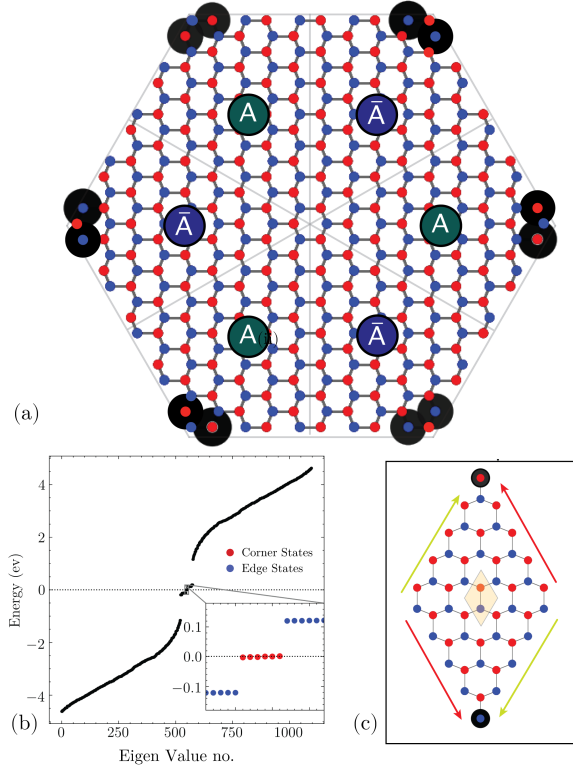


FIG. 3: (a) Finite size fragment of honeycomb (red and blue circles show Sb atoms below and above the plane), large black circles represent $|\psi|^2$ for the localized corner states indicated in in the eigenvalue spectrum in (b).

portant indicator becomes $[M_{\pm}^{(i)}]$ which is the difference in number of bands with even/odd character under the inversion operation at M and at Γ . We can see from the symmetry labeling in Figure 2(a) that the $[M_{\pm}^{(i)}] = \pm 2$. According to Table I in 17, the invariants at \bar{K} and M are either (2,0),(0,2) or (0,0) where the last case is the trivial topology. Thus, our system corresponds to the $h_{3c}^{(6)}$ primitive generator class in Benalcazar *et al.*'s notation. This indeed means that there are 3 filled bands and that the generator is obtained from orbitals centered at the Wyckoff position c . In the buckled Sb system, the space group is $P\bar{3}c1$ or D_{3d}^3 or #164 and the Wyckoff position is d . Thus, generalizing their notation our primitive generator would be $h_{3d}^{(3)}$ but in terms of charge fractionalization and polarization would have the same invariants as $h_{3c}^{(6)}$. (For the Kekulé case, the plane space group is $p3m1$ and the Wyckoff position is c .) It implies that there is no net dipole in the plane and the corner charge fractionalization will be $e/2$ in each $\pi/6$ sector.

We verify this prediction in Figure 3. The calculation is performed on a hexagonal 0D flake within the $\{p_x, p_y, p_z\}$ NN-TB Hamiltonian (rather than the simplified Kekulé model, which is however topologically equivalent). The eigenvalues of this Hamiltonian are shown in Fig. 3(b).

One can see that near zero energy, in the band gap there occurs both edge states (blue dots in inset of (b)) as well as mid-gap corner states (red). Their wave function modulo squared is indicated by the black circles in Fig. 3(a) clearly showing that these states are localized on the corner atoms. The $\pi/6$ sectors are labeled alternating A and \bar{A} , which are related by the inversion symmetry. One should note that though the existence of such corner states is deeply tied to the choice of symmetric unit cell, $\pi/6$ charge-fractionalization is not. In any general S_6 symmetric 0D fragment, one is guaranteed $e/2$ charge-fractionalization (other examples are given in SM).[22]

Relation to multipole insulators - A closely related point of view on the origin of the corner states arises in the context of quantized multipole insulators. Although the net polarization in the plane is zero for our case, the system has a non-zero quadrupole insulator character.

For a system with inversion symmetry, the contribution to the polarization projected on direction i from band n can be obtained from the the eigenvalues of the inversion operator at Time Reversal Invariant Momentum (TRIM) points M and Γ and is given by [4, 27, 29]

$$P_i^n = \frac{e}{2}(q_i^n \bmod 2) \quad \text{with} \quad (-1)^{q_i^n} = \frac{\eta_n(M_i)}{\eta_n(\Gamma)} \quad (1)$$

where $\eta^n(\mathbf{k})$ is the eigenvalue of the inversion operation. The quadrupole moment is then given by

$$Q_{ij} = \sum_n \frac{P_i^n P_j^n}{e} \quad (2)$$

For our system $(P_1^n, P_2^n) = (0, 0), (\frac{e}{2}, \frac{e}{2}), (\frac{e}{2}, \frac{e}{2})$ for bands $n = 1, 2, 3$ numbered from bottom to top. Thus the net dipole moment is trivially (e, e) as it should be for a $C_6(S_6)$ symmetric system but the net quadrupole moment has magnitude $e/2$, the effect of which can be seen in a $d-2$ system cut along the lattice vectors as shown in Fig. 3(c). In this figure we see the dipoles on opposite edges canceling each other but leading to a net quadrupole with charge accumulation at the two corners indicated by the black circles showing $|\Psi|^2$ of the corner localized state in the TB model. Not surprisingly, given the close connection pointed out earlier, similar corner states and quadrupole character are also found for the Kekulé lattice in the non-trivial limit.[29] Furthermore we note that not only regularly shaped fragments as considered here host such corner localized states, but more generally shaped 0D objects can host localized states on the perimeter when points on opposite sides are related by inversion symmetry. Examples are shown in SM.[22]

Robustness against disorder - It is important to note that the even though our system is a Topological Crystal Insulator (TCI), which are strictly speaking only weakly protected, the corner states are fairly robust to bulk disorder as shown in SM.[22] We show this numerically by

adding uniformly distributed random on-site bulk terms in a range of the magnitude of the band gap. This does confirm that approximate symmetries that are preserved on average are enough to host the fractional charges. But as soon as one perturbs the edges, the corner fractionalization gets destroyed. However, because of the existence of edge states in the corresponding higher dimensional 1D system, one still preserves the edge modes in the disordered system with perturbed edge states.

Conclusion - In this paper we report a physical condensed matter nanoscale realization of higher order topological insulator states, namely in the 2D system of buckled monolayer β -Sb (or other group-V atoms), which has already been experimentally fabricated although its topological features have not been reported yet. By examining the Wannier centers in this system to be localized on the bond centers, rather than the atoms, we have shown that this system is a topological crystal insulator supporting weak topological edge states. Because of the overall S_6 symmetry and its non-zero quadrupole character, it was shown by a slight generalization of the symmetry analysis of Ref. 17 to host topologically protected corner states, similar to those occurring in the Kekulé lattice.

Acknowledgements - This work was supported by the U.S. Department of Energy-Basic Energy Sciences under grant No. DE-SC0008933. The calculations made use of the High Performance Computing Resource in the Core Facility for Advanced Research Computing at Case Western Reserve University.

* Corresponding author: srr70@case.edu

† walter.lambrecht@case.edu

- [1] W. A. Benalcazar, B. A. Bernevig, and T. L. Hughes, *Science* **357**, 61 (2017), <https://science.sciencemag.org/content/357/6346/61.full.pdf>.
- [2] J. Langbehn, Y. Peng, L. Trifunovic, F. von Oppen, and P. W. Brouwer, *Phys. Rev. Lett.* **119**, 246401 (2017).
- [3] Z. Song, Z. Fang, and C. Fang, *Phys. Rev. Lett.* **119**, 246402 (2017).
- [4] W. A. Benalcazar, B. A. Bernevig, and T. L. Hughes, *Phys. Rev. B* **96**, 245115 (2017).
- [5] F. Schindler, A. M. Cook, M. G. Vergniory, Z. Wang, S. S. P. Parkin, B. A. Bernevig, and T. Neupert, *Science Advances* **4** (2018), 10.1126/sciadv.aat0346, <https://advances.sciencemag.org/content/4/6/eaat0346.full.pdf>.
- [6] F. Schindler, Z. Wang, M. G. Vergniory, A. M. Cook, A. Murani, S. Sengupta, A. Y. Kasumov, R. Deblock, S. Jeon, I. Drozdov, H. Bouchiat, S. Guéron, A. Yazdani, B. A. Bernevig, and T. Neupert, *Nature Physics* **14**, 918 (2018).
- [7] C. Yue, Y. Xu, Z. Song, H. Weng, Y.-M. Lu, C. Fang, and X. Dai, *Nature Physics* **15**, 577 (2019).
- [8] Z. Wang, B. J. Wieder, J. Li, B. Yan, and B. A. Bernevig, *Phys. Rev. Lett.* **123**, 186401 (2019).
- [9] F. Tang, H. C. Po, A. Vishwanath, and X. Wan, *Nature Physics* **15**, 470 (2019).
- [10] M. Ezawa, *Phys. Rev. B* **97**, 241402 (2018).
- [11] M. Ezawa, *Phys. Rev. Lett.* **120**, 026801 (2018).
- [12] S. Imhof, C. Berger, F. Bayer, J. Brehm, L. W. Molenkamp, T. Kiessling, F. Schindler, C. H. Lee, M. Greiter, T. Neupert, and R. Thomale, *Nature Physics* **14**, 925 (2018).
- [13] T. Kariyado and X. Hu, *Scientific Reports* **7**, 16515 (2017).
- [14] H. Xue, Y. Yang, F. Gao, Y. Chong, and B. Zhang, *Nature Materials* **18**, 108 (2019).
- [15] Z. Yan, *Phys. Rev. B* **100**, 205406 (2019).
- [16] J. Ji, X. Song, J. Liu, Z. Yan, C. Huo, S. Zhang, M. Su, L. Liao, W. Wang, Z. Ni, Y. Hao, and H. Zeng, *Nature Communications* **7**, 13352 (2016).
- [17] W. A. Benalcazar, T. Li, and T. L. Hughes, *Phys. Rev. B* **99**, 245151 (2019).
- [18] S. K. Radha and W. R. L. Lambrecht, “Topological band structure transitions in honeycomb antimonene as function of buckling,” (2019), arXiv:1912.03755 [cond-mat.mtrl-sci].
- [19] P. E. Blöchl, *Phys. Rev. B* **50**, 17953 (1994).
- [20] P. Giannozzi, S. Baroni, N. Bonini, M. Calandra, R. Car, C. Cavazzoni, D. Ceresoli, G. L. Chiarotti, M. Cococcioni, I. Dabo, A. D. Corso, S. de Gironcoli, S. Fabris, G. Fratesi, R. Gebauer, U. Gerstmann, C. Gougoussis, A. Kokalj, M. Lazzeri, L. Martin-Samos, N. Marzari, F. Mauri, R. Mazzarello, S. Paolini, A. Pasquarello, L. Paulatto, C. Sbraccia, S. Scandolo, G. Schläuzer, A. P. Seitsonen, A. Smogunov, P. Umari, and R. M. Wentzcovitch, *Journal of Physics: Condensed Matter* **21**, 395502 (2009).
- [21] G. Pizzi, V. Vitale, R. Arita, S. Blügel, F. Freimuth, G. Géranton, M. Gibertini, D. Gresch, C. Johnson, T. Koretsune, J. Ibañez-Azpiroz, H. Lee, J.-M. Lihm, D. Marchand, A. Marrazzo, Y. Mokrousov, J. I. Mustafa, Y. Nohara, Y. Nomura, L. Paulatto, S. Poncé, T. Ponweiser, J. Qiao, F. Thöle, S. S. Tsirkin, M. Wierzbowska, N. Marzari, D. Vanderbilt, I. Souza, A. A. Mostofi, and J. R. Yates, *Journal of Physics: Condensed Matter* **32**, 165902 (2020).
- [22] Supplemental material contains computational details, including the various tight-binding models used, figures of the (anti)Kagome lattice of (anti)bond centers, differently shaped 0D fragments and the robustness of the edge states and band structures and is available at the publication URL.
- [23] B. Bradlyn, L. Elcoro, J. Cano, M. G. Vergniory, Z. Wang, C. Felser, M. I. Aroyo, and B. A. Bernevig, *Nature* **547**, 298 (2017).
- [24] J. Cano, B. Bradlyn, Z. Wang, L. Elcoro, M. G. Vergniory, C. Felser, M. I. Aroyo, and B. A. Bernevig, *Phys. Rev. B* **97**, 035139 (2018).
- [25] M. van Schilfhaarde, T. Kotani, and S. Faleev, *Phys. Rev. Lett.* **96**, 226402 (2006).
- [26] L.-H. Wu and X. Hu, *Scientific Reports* **6**, 24347 (2016).
- [27] F. Liu and K. Wakabayashi, *Phys. Rev. Lett.* **118**, 076803 (2017).
- [28] F. Liu, M. Yamamoto, and K. Wakabayashi, *Journal of the Physical Society of Japan* **86**, 123707 (2017).
- [29] F. Liu, H.-Y. Deng, and K. Wakabayashi, *Phys. Rev. Lett.* **122**, 086804 (2019).

- [30] W. P. Su, J. R. Schrieffer, and A. J. Heeger, Phys. Rev. Lett. **42**, 1698 (1979).
- [31] J. Ji, X. Song, J. Liu, Z. Yan, C. Huo, S. Zhang, M. Su, L. Liao, W. Wang, Z. Ni, Y. Hao, and H. Zeng, Nature Communications **7**, 13352 (2016).
- [32] J. P. Perdew, K. Burke, and M. Ernzerhof, Phys. Rev. Lett. **77**, 3865 (1996).
- [33] D. Pashov, S. Acharya, W. R. Lambrecht, J. Jackson, K. D. Belashchenko, A. Chantis, F. Jamet, and M. van Schilfgaarde, Computer Physics Communications **219**, 107065 (2019).
- [34] T. Kotani, M. van Schilfgaarde, and S. V. Faleev, Phys. Rev. B **76**, 165106 (2007).
- [35] L. Hedin, Phys. Rev. **139**, A796 (1965).
- [36] L. Hedin and S. Lundqvist, in *Solid State Physics, Advanced in Research and Applications*, Vol. 23, edited by F. Seitz, D. Turnbull, and H. Ehrenreich (Academic Press, New York, 1969) pp. 1–181.
- [37] M. Methfessel, M. van Schilfgaarde, and R. A. Casali, in *Electronic Structure and Physical Properties of Solids. The Use of the LMTO Method*, Lecture Notes in Physics, Vol. 535, edited by H. Dreyssé (Berlin Springer Verlag, 2000) p. 114.
- [38] T. Kotani and M. van Schilfgaarde, Phys. Rev. B **81**, 125117 (2010).
- [39] <http://www.questaal.org>.

SUPPLEMENTAL MATERIAL

Computational Methods

The band structure calculations of the 2D periodic system were performed using density functional theory in the Perdew-Burke-Ernzerhof (PBE)[32] generalized gradient approximation (GGA) both in the full potential linearized muffin-tin orbital method[33] and using a plane wave projector augmented wave method (PAW).[19] The band structure of the 2D buckled honeycomb monolayer of Sb in Fig.2 of the main paper was done using the quasiparticle self-consistent QSGW many-body perturbation theory method.[25, 34] Here *GW* stands for the one-electron Green's function and *W* for the screened Coulomb interaction.[35, 36] These calculations were performed using the full-potential linearized muffin-tin orbital (FP-LMTO) method[37, 38] using the questaal package, which is fully described in Ref.[33] and available at [39]. Convergence parameters were chosen as follows: basis set *spdf* – *spd* spherical wave envelope functions plus augmented plane waves with a cut-off of 3 Ry, augmentation cutoff $l_{max} = 4$, **k**-point mesh, $12 \times 12 \times 2$. The monolayer slabs were separated by a vacuum region of 3 nm. In the *GW* calculations the self energy Σ is calculated on a **k**-mesh of $5 \times 5 \times 2$ points and interpolated to the above finer mesh and the bands along symmetry lines.

Tight binding calculations were used for the nanoribbons or finite size fragments. We used both a nearest neighbor tight-binding model as described in Ref. 18 or

a Wannier interpolation [21] of the DFT band structure obtained from Quantum Espresso [20] with kinetic energy cutoff of 50 Ry.

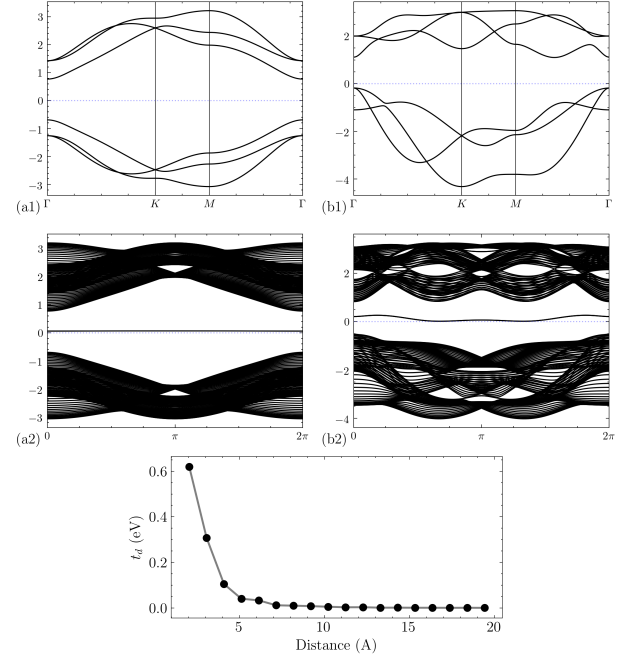


FIG. 4: (top) (a1) (a2) Wannier interpolated LDA bands with *N.N* interaction and corresponding 1D bands (b1) (b2) same as above with *N.N.N*. (bottom) Wannier interaction strength as function of distance.

Figure 4 shows the 2D and nanoribbon band structures obtained within this TB model with either nearest neighbor (NN) or next nearest neighbor (NNN) hopping integrals as well as the decay of the hopping parameters. It is found that the NNN model already reproduces the full DFT plane wave results adequately. The NN model is seen to have particle hole symmetry, meaning that the eigenvalues occur in pairs $\pm |E_{n\mathbf{k}}|$. It also shows a completely dispersionless edge band while in the NNN model the edge band shows a small amount of dispersion. The nanoribbon band structure of Fig. 1 in the main paper was done with this NNN Hamiltonian. The eigenvalues of the 0D nanofragments were done with the NN TB Hamiltonian introduced in Ref. 18 which is shown below to be close to the NN version of this Wannier extracted Hamiltonian. In any case, all these Hamiltonians are topologically equivalent. Tests of the main features with NNN TB Hamiltonians for 0D systems were also done but do not produced qualitative changes to the conclusions.

In Figure 5 we show a further comparison of the DFT, Wannier NN and two other models. The one labeled H_p corresponds to the NN-TB model used in 18. This model uses $\{p_x, p_y, p_z\}$ orbitals and the standard Slater-Koster two-center approximation to write the hopping integrals in terms of $V_{pp\sigma}$ and $V_{pp\pi}$ interactions. This allowed us to

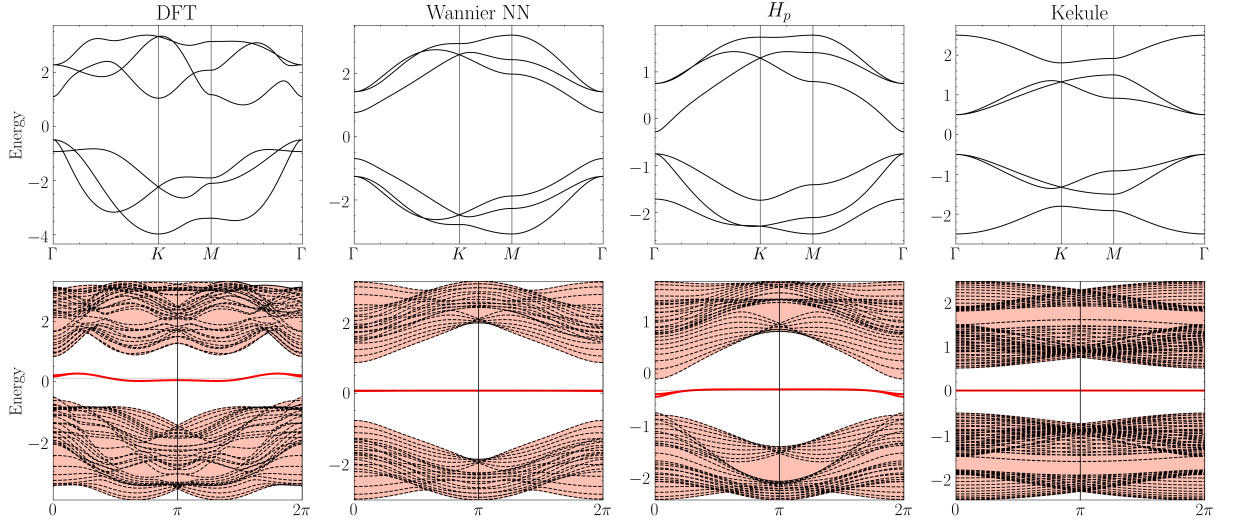


FIG. 5: Bulk and edge band structures at different level of theories

follow the behavior as function of buckling angle, assuming the relative amount of $V_{pp\sigma}$ $V_{pp\pi}$ depend only on angle but the bond lengths and hence the $V_{pp\sigma}$ and $V_{pp\pi}$ two-center integrals themselves stayed fixed. In this model, also the p_x, p_y orbital energies are slightly displaced in energy from the p_z orbitals thereby breaking the particle-hole symmetry. Although there are changes in the ordering of bands within the occupied manifold, and within the unoccupied manifold, the set of irreducible representations comprising the VB and CB manifolds stay the same and this is the only feature that matters for the topological aspects discussed in the main paper. Finally, we show in this figure the results of the band structure of the Kekulé model, whose tight-binding Hamiltonian can be written.

$$H = \begin{pmatrix} 0 & \delta & 0 & e^{i\mathbf{k}\cdot\mathbf{a}_3} & 0 & 1 \\ \delta & 0 & 1 & 0 & e^{i\mathbf{k}\cdot\mathbf{a}_2} & 0 \\ 0 & 1 & 0 & \delta & 0 & e^{i\mathbf{k}\cdot\mathbf{a}_1} \\ e^{-i\mathbf{k}\cdot\mathbf{a}_3} & 0 & \delta & 0 & 1 & 0 \\ 0 & e^{-i\mathbf{k}\cdot\mathbf{a}_2} & 0 & 1 & 0 & \delta \\ 1 & 0 & e^{-i\mathbf{k}\cdot\mathbf{a}_1} & 0 & \delta & 0 \end{pmatrix} \quad (3)$$

where $\mathbf{a}_1 = (1, 0)$, $\mathbf{a}_2 = (\frac{1}{2}, \frac{\sqrt{3}}{2})$. The Kekulé orbital centers are numbered 1-6 in Fig.2(c) in the main text and the lattice vectors are indicated by blue arrows.

Kagome and Anti-kagome

Figure 6 show how the bond centers form a Kagome lattice and the antibond centers form what we call here an anti-Kagome lattice. The filled and open circles are the Sb atoms point up or down the plane of the projection plane the corners of the pink triangles are the bond

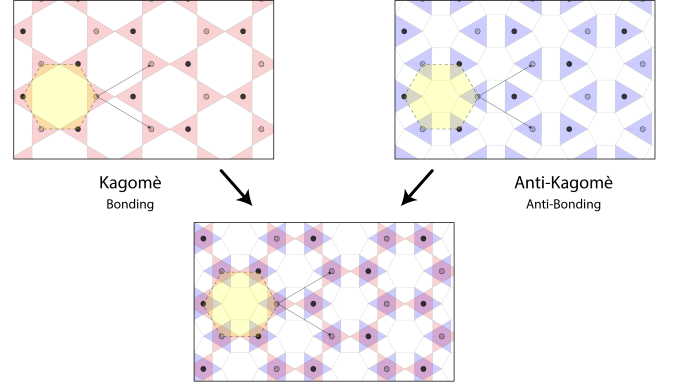


FIG. 6: Bonding and Anti bonding states forming Kagome and Anti kagome

centers and form a Kagome lattice. On the right, the blue triangle corners are at the anti-bond centers and form a distinct lattice which we call here anti-Kagome. Both are shown superposed on each other in the bottom figure.

$(d-2)$ states and symmetry

In the main text, we used either a perfectly hexagonal 0D model or an integer multiple of the 2D primitive unit cell given by the $\mathbf{a}_1, \mathbf{a}_2$ lattice vectors. This lead to symmetrically distributed corner localized states within each $\pi/6$ sector or a quadrupole symmetry showing charge localization. However more generally localized states at the edges can be obtained from other 0D fragments as illustrated here in Figure 7. These states generally occur at edge points related to another point on the circumference

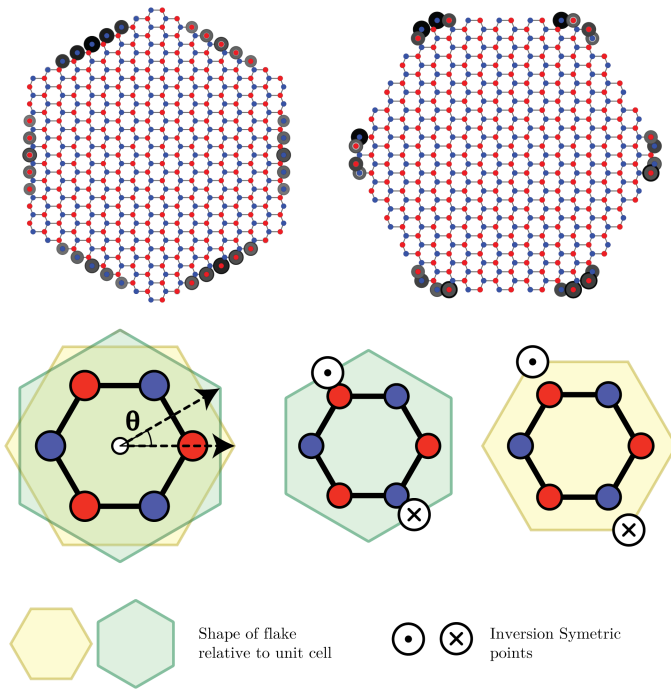


FIG. 7: Different C_6 symmetric flake geometry and the mid gap state wavefunction

of the 0D system by inversion symmetry. In the figure on the left we see edge states localized on zigzag edges but not on the corners joining them, while on the right we see states localized at the corners joining arm-chair edges. The figures below illustrate the relation between the overall 0D nanoscale fragment and the lattice unit cell and

which points are related by inversion which is the key crystallographic symmetry protecting these topological features.

Disorder effects

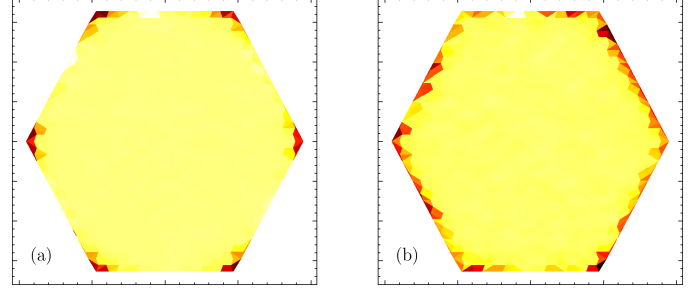


FIG. 8: Total charge distribution of occupied states with on-site potential added stochastically from a uniform distribution of $[-\frac{E_g}{2}, \frac{E_g}{2}]$ (a) everywhere except edge atoms (b) everywhere

Figure 8 shows the total charge distribution in a C_6 symmetric D0 system made up of 4200 sites $\times 3 = 12600$ orbitals. Random on-site potential sampled from a uniform distribution in the interval $[-\frac{E_g}{2}, \frac{E_g}{2}]$ (where E_g is the band gap) was added on (a) all atoms other than the edges (b) everywhere uniformly. Both simulations were run 500 times and the average charge density is plotted. This shows that bulk disorder does not destroy the corner states while disorder also at the edges does destroy the corner states but still shows localized states along the edges.